

Dynamically generated synthetic electric fields for photonsPetr Zapletal^{1,2}, Stefan Walter,^{2,3} and Florian Marquardt^{2,3}¹*Cavendish Laboratory, University of Cambridge, Cambridge CB3 0HE, United Kingdom*²*Max Planck Institute for the Science of Light, Staudtstraße 2, 91058 Erlangen, Germany*³*Institute for Theoretical Physics, University Erlangen-Nürnberg, Staudtstraße 7, 91058 Erlangen, Germany*

(Received 18 July 2018; published 6 August 2019)

Static synthetic magnetic fields give rise to phenomena including the Lorentz force and the quantum Hall effect even for neutral particles, and they have by now been implemented in a variety of physical systems. Moving toward fully dynamical synthetic gauge fields allows, in addition, for backaction of the particles' motion onto the field. If this results in a time-dependent vector potential, conventional electromagnetism predicts the generation of an electric field. Here, we show how synthetic electric fields for photons arise self-consistently due to the nonlinear dynamics in a driven system. Our analysis is based on optomechanical arrays, where dynamical gauge fields arise naturally from phonon-assisted photon tunneling. We study open, one-dimensional arrays, where synthetic magnetic fields are absent. However, we show that synthetic electric fields can be generated dynamically. The generation of these fields depends on the direction of photon propagation, leading to a mechanism for a photon diode, inducing nonlinear unidirectional transport via dynamical synthetic gauge fields.

DOI: [10.1103/PhysRevA.100.023804](https://doi.org/10.1103/PhysRevA.100.023804)**I. INTRODUCTION**

The field of cavity optomechanics, addressing the interaction between light and sound, has made rapid strides in recent years [1]. Experiments have shown ground-state cooling [2,3], measurements of motion with record sensitivity [4], efficient conversion between microwave and optical photons [5], dynamics of vibrations near exceptional points [6], and the control of single phonons [7], to name but a few achievements.

Due to the optomechanical interaction, mechanical vibrations can change light frequency. During this process, the mechanical oscillation phase is imparted onto the light field. This provides a natural means to generate synthetic magnetic fields for photons, as was first suggested in Refs. [8,9]. Together with reservoir engineering [10], these ideas form the theoretical basis underlying a recent series of pioneering experiments on optomechanical nonreciprocity [11–16]. While those still operate in few-mode setups, future extensions to optomechanical arrays [17–20] will enable studying photon transport on a lattice in the presence of an arbitrary tunable synthetic magnetic field [9]. A similar optomechanical design underlies the first proposal for engineered topological phonon transport [21]. These developments tie into the wide field of synthetic magnetic fields and topologically protected nonreciprocal transport, first envisaged and implemented for cold atoms [22–25] and then for photons [26–32], phonons [21,33–38], and other platforms [39,40].

In these works, gauge fields are fixed by external parameters, e.g., the phases of external driving beams. It was understood only recently that optomechanics provides a very natural platform for creating dynamical classical gauge fields [41]: if the mechanical resonator is not periodically modulated by external driving but rather undergoes limit-cycle oscillations, the phase of those oscillations becomes a dynamical gauge field. This field is a new degree of freedom that can be influenced by photons.

The theory of *classical* dynamical gauge fields is not only important as a starting point for high-energy *quantum* field theory (e.g., Yang-Mills and Higgs theories [42–44]), but is also an active area of research in modern condensed matter physics (e.g., in the gauge theory of dislocations [45], spin ice [46], and nematic liquid crystals [47,48]). We emphasize that our main goal is different from the attempts to build quantum simulators for existing high-energy gauge theories (suggested theoretically for ultracold atoms in optical lattices [49,50], superconducting circuits [51,52], cavity quantum electrodynamics [53], and trapped ions [54]), where the experimental implementation remains very challenging (see Ref. [55] for the first steps). Rather, our work provides insights for all physical systems where limit-cycle oscillators assist transitions between linear modes, by connecting these systems to the general mathematical framework of classical dynamical gauge fields. This includes different kinds of limit cycles (electrical, mechanical, optical, and spin oscillators, pumped using electrical feedback, optomechanical backaction, etc.), different kinds of linear modes (microwave, mechanical, optical, magnon resonances, etc.), and almost arbitrary nonlinear coupling, using optical or mechanical nonlinearities, Josephson junctions, etc. For concreteness, we describe it here for the case of optomechanics, but the mathematics and the predictions are general and of wide experimental applicability.

Published by the American Physical Society under the terms of the Creative Commons Attribution 4.0 International license. Further distribution of this work must maintain attribution to the author(s) and the published article's title, journal citation, and DOI.

If the gauge field dynamics results in a time-dependent vector potential, conventional electromagnetism dictates that this describes an electric field. In this work, we predict that synthetic electric fields can arise in elementary optomechanical systems, in a dynamical way. The scenarios in which these electric fields arise, and their physical consequences, are qualitatively different from the more conventional self-consistently generated magnetic fields discussed in our previous work [41]. They can arise even in a linear arrangement of coupled photon modes, where static vector potentials do not have any effect, since they can be gauged away. This makes them a very relevant phenomenon for present-day experimental implementations, in setups as simple as two coupled optical modes. Moreover, the appearance of electric fields turns out to depend on the direction of photon propagation. In this way, we uncover a mechanism for nonlinear unidirectional transport of photons (a photon diode). This works especially well in arrays, where transport is significantly suppressed in the blockaded direction.

Synthetic electric fields for photons have been previously analyzed only in the context of prescribed external driving [56,57], i.e., not dynamically generated. In these cases, the nonlinear dynamics and unidirectional transport explored in our work are absent.

II. DYNAMICAL GAUGE FIELDS FOR PHOTONS

The optomechanical interaction can be used to realize phonon-assisted photon tunneling, which, as we have shown previously, offers a natural route toward classical dynamical gauge fields for photons [41]. Photons hopping between optical modes \hat{a}_1 and \hat{a}_2 absorb or emit a phonon from a mechanical mode \hat{b} . A pictorial representation of this process is shown in Fig. 1(b). Many implementations are conceivable (photonic crystal devices, coupled toroids, and microwave circuits [1]), but a suitable realization might simply consist of the well-known membrane-in-the-middle setup [58,59]. The Hamiltonian is

$$\hat{H} = \sum_{j=1}^2 \nu_j \hat{a}_j^\dagger \hat{a}_j + \Omega \hat{b}^\dagger \hat{b} + J(\hat{b} \hat{a}_2^\dagger \hat{a}_1 + \text{H.c.}), \quad (1)$$

where ν_j are the optical frequencies of modes \hat{a}_j , Ω is the frequency of the mechanical oscillator, and J is the tunneling amplitude [41]. In the following, we set $\hbar = 1$. The optical frequencies are detuned from one another to suppress direct tunneling between the optical modes. The phonon-assisted photon tunneling is selected by tuning the mechanical frequency, $\Omega \approx |\nu_2 - \nu_1|$. The Hamiltonian (1) is valid within the rotating-wave approximation for $\nu_2 > \nu_1$ and $\Omega \gg \kappa, J, JB$, where κ is the photon decay rate and B is the amplitude of the mechanical oscillations: $\langle \hat{b} \rangle = B e^{i\phi} e^{-i\Omega t}$.

During the photon tunneling process $\hat{b} \hat{a}_2^\dagger \hat{a}_1$, the mechanical phase ϕ is imprinted on the photons, similar to an Aharonov-Bohm (Peierls) phase. This can be used for optomechanical generation of static gauge fields, as proposed in Ref. [9], and the scheme can be readily implemented in optomechanical crystals [60,61] or the membrane-cavity setup [58,59,62]. It was experimentally realized in Ref. [14].

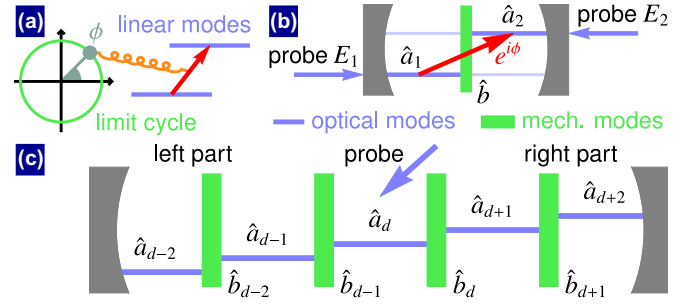


FIG. 1. Setup exhibiting dynamically generated synthetic electric fields. (a) In general terms: Limit-cycle oscillator assisting the transition between linear modes. (b) Optomechanical realization: A cavity with a movable membrane (green rectangle) in the middle supporting optical supermodes \hat{a}_1 and \hat{a}_2 (mostly localized left and right, respectively). The mechanical mode \hat{b} undergoes limit-cycle oscillations. Photons tunneling (red arrow) from optical mode \hat{a}_1 to \hat{a}_2 absorb a phonon from the mechanical oscillation, thereby acquiring a phase shift set by the oscillation phase ϕ . Photon transport through the setup can be probed by driving mode \hat{a}_1 or \hat{a}_2 . Optical frequencies are represented by the blue lines. (c) A one-dimensional array, with optical modes \hat{a}_j of increasing frequency. Mechanical modes \hat{b}_j assist tunneling between modes \hat{a}_j and \hat{a}_{j+1} . Some mode, \hat{a}_d , is driven by a laser (blue arrow), probing photon transport both toward the left and right.

To implement dynamical gauge fields for photons, i.e., fields that are themselves dynamical degrees of freedom, the oscillation phase ϕ (the “gauge field”) has to evolve freely, which is the case if the mechanical mode performs limit-cycle oscillations [41]. The limit-cycle oscillations can be generated by pumping an ancillary optical mode, situated at a different frequency, on the blue sideband [63]. This pumping does not impose any particular phase on the mechanical oscillator and thus the phase is able to evolve according to its own dynamics. In this way, the phase ϕ turns into a dynamical gauge field, being influenced by photon transport and acting back on photons. The system of Eq. (1) can be used as a building block for optomechanical arrays with dynamical gauge fields for photons, as we first proposed in Ref. [41]. We use the equations of Ref. [41] as our starting point, to predict the phenomenon of synthetic electric fields generated by nonlinear dynamics, giving rise to unidirectional photon transport.

III. THE BASIC PHYSICS BEHIND OUR RESULTS

We start with a preview of our results, emphasizing the physical intuition. Any oscillator driven by a resonant force $F_0 \cos(\Omega t - \theta)$ experiences a drift, $\dot{\phi} \propto F_0 \cos(\phi - \theta)$, of its phase ϕ . In our case, the force is the radiation pressure oscillating at the beat note between the two optical modes, and we obtain $\dot{\phi} = -(J/B)|a_1||a_2| \cos(\phi - \theta)$, where θ is the phase difference between the optical modes. If the forcing phase θ is kept constant, this results in a stable fixed point $\phi = \theta - \pi/2$. For a limit-cycle oscillator, that behavior is known as phase locking (injection locking) to an external drive (see Appendix D for more details).

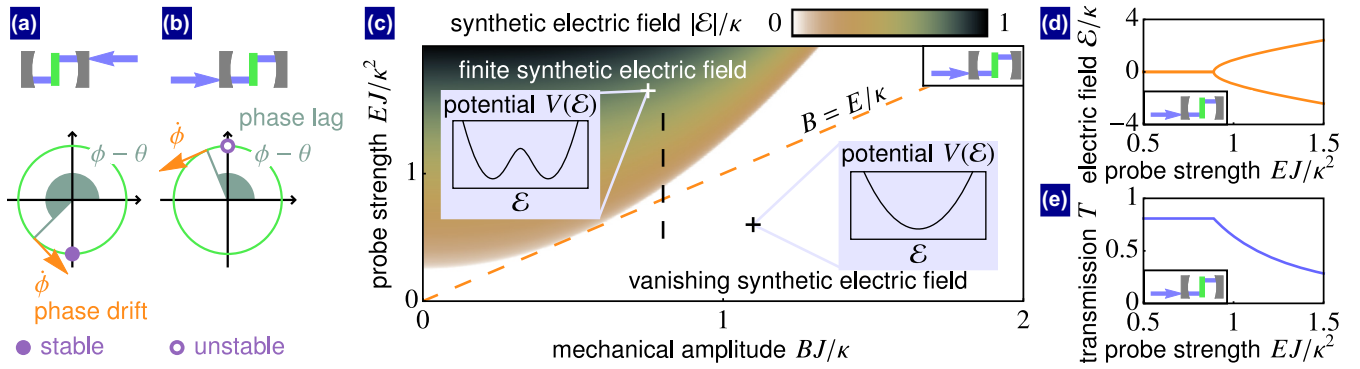


FIG. 2. Dynamically generated synthetic electric fields in the two-site system. (a), (b) Phase evolution on the mechanical limit cycle (green orbit). (a) When the higher-frequency optical mode is laser-driven, the system settles into a stable fixed point, with a phase lag $\phi - \theta = -\pi/2$. (b) When the lower-frequency optical mode is driven, the phase is continuously repelled from an unstable fixed point $\phi - \theta = +\pi/2$, generating a finite synthetic electric field $\mathcal{E} = \dot{\phi} \neq 0$ acting on the photons. (c) The phase diagram. In the white region, \mathcal{E} vanishes in the steady state. If the lower-frequency mode, a_1 , is driven, \mathcal{E} bifurcates in the colored region to finite steady-state values. Their absolute values are indicated by the color scale. The blue insets show the effective potential $V(\mathcal{E})$ determining the steady-state value of \mathcal{E} . The dashed black line denotes the cut along which \mathcal{E} and the optical transmission T are plotted in (d) and (e), respectively. For the higher-frequency mode, a_2 , being driven, \mathcal{E} always vanishes for any values of the system parameters. Consequently, the transmission is never suppressed.

However, in our case an interesting self-consistency problem arises: the phase difference $\theta = \theta_2 - \theta_1$ of the two optical modes depends on ϕ itself, as the phase ϕ is imprinted onto the photons during the phonon-assisted photon tunneling. The phase of the force thus follows the oscillation phase. We now discuss qualitatively the resulting physics, which will be bolstered by detailed analysis later. Two cases need to be distinguished, depending on which optical mode is driven by the laser [see Figs. 2(a) and 2(b)]. If the higher-frequency optical mode (labeled “2”) is driven, then we find $\theta = \phi + \pi/2$. The crucial term $\pi/2$ comes about due to the resonant excitation of the lower-frequency mode via the phonon-assisted transition $2 \rightarrow 1$. Comparing with the stable fixed point for ϕ deduced above, we conclude that any value of ϕ is now stable.

The situation drastically changes if the lower-frequency optical mode is driven by the laser. Then, we find $\theta = \phi - \pi/2$, where the sign has flipped because the roles of optical modes have been interchanged (now the higher-frequency mode is excited by the phonon sideband of the driven lower-frequency mode). This corresponds to an unstable fixed point. Once ϕ tries to move away, θ will follow, such that ϕ is forever repelled. This results in a finite phase drift $\dot{\phi} \neq 0$, corresponding to an effective shift of the mechanical frequency. Thus, the phonon-assisted tunneling process toward the higher optical mode is no longer in resonance but detuned by $\dot{\phi}$. This off-resonant excitation shifts the optical phase difference according to $\theta \approx \phi - \pi/2 - \dot{\phi}/(\kappa/2)$. The equation $\dot{\phi} \propto -\cos(\phi - \theta)$ can then be fulfilled at a certain value of $\dot{\phi}$, which has to be obtained self-consistently. This is the qualitative origin of the nonlinear dynamics that gives rise to what we will identify below as a synthetic electric field $\mathcal{E} = \dot{\phi}$ acting on photons.

IV. DYNAMICS AND SYNTHETIC ELECTRIC FIELDS

Let us analyze the dynamics of the two-site system (1) with the mechanical oscillator performing limit-cycle oscillations. The optical mode \hat{a}_j is driven by a laser of amplitude

E_j at frequency $\nu_{D,j}$, probing photon transport through the system. The optical and mechanical amplitudes are assumed large such that quantum noise can be neglected, which is an excellent approximation for all existing optomechanical experiments studying nonlinear dynamics.

Following Ref. [41], the classical equations of motion for the optical amplitudes $a_j = \langle \hat{a}_j \rangle$ and the mechanical phase ϕ read

$$\dot{\phi} = \Delta_M - \frac{J}{B} \text{Re}[a_1^* a_2 e^{-i\phi}], \quad (2)$$

$$\dot{a}_1 = i\Delta_1 a_1 - iE_1 - iJBe^{-i\phi} a_2 - \frac{\kappa}{2} a_1, \quad (3)$$

$$\dot{a}_2 = i\Delta_2 a_2 - iE_2 - iJBe^{i\phi} a_1 - \frac{\kappa}{2} a_2, \quad (4)$$

where $\Delta_j = \nu_{D,j} - \nu_j$ and $\Delta_M = \nu_{D,2} - \nu_{D,1} - \Omega$ are optical and mechanical detunings, respectively (switching to suitable rotating frames). The mechanical amplitude B is considered fixed. These equations form the starting point of our analysis.

If only one optical mode is driven, no external phase is imprinted. The mechanical oscillator is free to pick any phase despite the interaction with the optical modes. The phase forms a classical gauge field with $U(1)$ symmetry. The gauge transformation

$$\phi \mapsto \phi + \chi_2 - \chi_1, \quad (5)$$

$$a_j \mapsto a_j e^{i\chi_j}, \text{ for } j = 1, 2, \quad (6)$$

generates a new valid solution of the dynamical equations, for any real functions $\chi_j(t)$. The transformation also preserves optical and mechanical frequencies whenever it is time-independent, i.e., $\chi_j = \text{constant}$. However, if χ_j are time-dependent, Eqs. (5) and (6) have to be supplemented by a shift in frequencies: $\Omega \mapsto \Omega + \dot{\chi}_1 - \dot{\chi}_2$ and $\nu_j \mapsto \nu_j - \dot{\chi}_j$. Any time-evolving phase ϕ can be viewed as generating a synthetic electric field

$$\mathcal{E} = \dot{\phi} \quad (7)$$

for photons. For example, if mode 1 is driven, we can re-gauge using $\chi_1 = 0$, $\chi_2 = -\phi$, which results in a description where the mechanical phase is static but $v_2 \mapsto v_2 + \mathcal{E}$. This describes an effective optical frequency shift, which can be interpreted as a synthetic electric field for photons in the same way that an energy difference between electronic levels indicates a voltage drop, i.e., a real electric field. In conventional electromagnetism, an electric field can be represented either as a time-dependent vector potential or a scalar potential gradient. Analogously, the synthetic electric field \mathcal{E} is described either by the time evolution of the mechanical phase or by an effective frequency shift. As we will show, \mathcal{E} has important consequences for photon transport.

V. DYNAMICAL PHASE DIAGRAM

Here, \mathcal{E} is not prescribed externally but it arises due to the dynamics of coupled optical and mechanical modes. The optical modes induce the force F acting on the mechanical phase. The resulting phase evolution may generate a field \mathcal{E} which effectively modifies the optical frequency difference and, consequently, the population of the optical modes.

The results of the dynamical analysis are shown in Fig. 2. The results were obtained by linear stability analysis and numerical simulations.

We consider the fully resonant situation where physical effects are most pronounced, as both optical driving and phonon-assisted photon tunneling are resonant ($\Delta_M = \Delta_1 = \Delta_2 = 0$). The system always converges to a steady state. The steady-state value of \mathcal{E} depends on two dimensionless parameters: the rescaled limit-cycle amplitude BJ/κ and the rescaled laser amplitude EJ/κ^2 .

The dynamical analysis becomes more intuitive by “integrating out” optical modes. This leaves us with an effective potential $V(\mathcal{E})$, whose minima determine steady-state values of \mathcal{E} (see Appendix B for the full analytical expression):

$$\dot{\mathcal{E}} = -\frac{dV(\mathcal{E})}{d\mathcal{E}} = 0. \quad (8)$$

In the white region of the phase diagram, Fig. 2(c), the potential $V(\mathcal{E})$ has a single minimum at $\mathcal{E} = 0$ (see the blue inset). For the lower-frequency mode, a_1 , being driven, this steady state becomes unstable in the colored region of the phase diagram, where the potential $V(\mathcal{E})$ has two minima at finite values of \mathcal{E} . The field \mathcal{E} can develop such a nonzero value for $B < E/\kappa$ (above the dashed orange line). In terms of physical parameters, the occupation of the driven optical mode has to exceed the phonon number in the limit-cycle oscillation. In contrast, if the higher-frequency mode, a_2 , is driven, $V(\mathcal{E})$ always has a single minimum at $\mathcal{E} = 0$ for any values of system parameters. The states are not qualitatively changed for finite mechanical and laser detunings (see Appendix B).

We now study effects of the dynamically generated synthetic electric field on light transport. The transmission T is the ratio of the output power leaking from the nondriven mode, $\kappa|a_2|^2$ (if mode 1 is driven) or $\kappa|a_1|^2$ (if mode 2 is

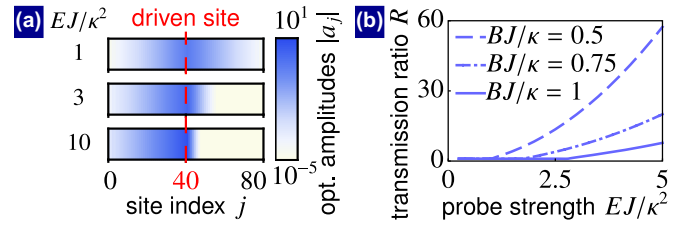


FIG. 3. Light transport in a 1D array with dynamical gauge fields and the generation of a barrier for photon transport induced by synthetic electric fields. (a) The optical amplitudes $|a_j|$ as a function of position for different values of the laser amplitude E and $BJ/\kappa = 1$ (shown on a logarithmic scale). The dashed red line denotes the driven site. Transport to the right is strongly suppressed. (b) The ratio $R = |a_{d-1}/a_{d+1}|^2$ of the optical amplitudes adjacent to the driven site $j = d$. (Plotted for $n = 81$ sites, site $d = 40$ being driven.)

driven), and the driving power E^2/κ . We find that

$$T = \frac{\frac{B^2 J^2}{\kappa^2}}{\left(\frac{B^2 J^2}{\kappa^2} + \frac{1}{4}\right)^2 + \frac{1}{4\kappa^2} \mathcal{E}^2} \quad (9)$$

is suppressed when a finite field \mathcal{E} detunes the tunneling process from resonance. In Figs. 2(d) and 2(e), \mathcal{E} and T , respectively, are depicted along the cut in Fig. 2(c) denoted by the dashed black line.

When light propagates to higher optical frequencies, the phonon-assisted photon tunneling is suppressed due to the synthetic electric field. In contrast, the field always vanishes when light propagates toward lower optical frequencies. In this way, dynamical gauge fields give rise to a mechanism for unidirectional light transport. In the following, we demonstrate this effect in one-dimensional arrays.

VI. NONLINEAR UNIDIRECTIONAL LIGHT TRANSPORT IN A ONE-DIMENSIONAL ARRAY

The physics of synthetic electric fields also affects photon transport in arrays [Fig. 1(c)]; for more details see Appendix E. Figure 3(a) shows the result for a 1D array: for a sufficiently large laser drive, the system switches into a state where finite \mathcal{E} develops to the right of the laser drive. This is the direction where photons need to gain energy when tunneling, and where we already saw in the two-site system that (i) a finite field can develop, and (ii) it suppresses photon transport. In the array, this results in a rapid exponential suppression of light intensity. In contrast, light easily propagates toward the left, where \mathcal{E} remains zero. In Fig. 3(b), we plot the ratio $R = |a_{d-1}/a_{d+1}|^2$ of transmission to the sites adjacent to the driven site $j = d$ as a function of EJ/κ^2 . The suppression of light propagation to the right, i.e., $R > 1$, is achieved above the threshold of the laser amplitude. At m sites distance from the driven site, the ratio is exponentially increased to R^m .

Our numerical simulations indicate that unidirectional light propagation can also be observed in two-dimensional square arrays. In the future, one might study how these phenomena affect synchronization dynamics of coupled optomechanical self-oscillators [18,64,65].

VII. EXPERIMENTAL PARAMETERS REQUIRED FOR GENERATING THE SYNTHETIC ELECTRIC FIELD

We estimate that unidirectional light transport can be observed for experimentally realistic parameters. For the membrane-in-the-middle setup, feasible parameters are $\kappa \approx 300$ kHz, $J \approx 1$ Hz, a zero-point fluctuation amplitude of $x_{\text{ZPF}} \approx 10^{-15}$ m, and a number of photons in the cavity $(E/\kappa)^2 \sim 10^{10}$ [59]. A typical phonon number in limit-cycle oscillations driven well above threshold is $B^2 \sim (\kappa/J)^2 \sim 10^{10}$ with a corresponding real oscillation amplitude $2x_{\text{ZPF}}B \sim 100$ pm [63]. Optical modes can be represented by hybridized modes of a cavity with avoided crossing [59]. The splitting of their frequencies ≈ 200 kHz can match the mechanical frequency. For these experimental parameters, $EJ/\kappa^2 \sim 1$ and $BJ/\kappa \sim 1$ are promising for observing unidirectional light transport (see Fig. 2). The phonon number can be decreased below the photon number in the driven mode by driving mechanical self-oscillations closer to threshold [63], fulfilling the necessary condition for a finite synthetic electric field (Fig. 2).

VIII. CONCLUSIONS

While synthetic gauge fields for photons have been investigated thoroughly in recent years, little has been known about the dynamical situation. In this work, we have uncovered how a synthetic electric field can be spontaneously created in a readily realizable optomechanical setup. The resulting nonlinear photon-diode type of unidirectional transport can lead to a large isolation ratio, especially in arrays. We demonstrate how the interplay of nonlinearity, dynamics, and artificial gauge fields can produce novel physical effects and possible new devices, which are not limited only to optomechanics but can be reached whenever a limit-cycle oscillator assists the transition between harmonic oscillators.

ACKNOWLEDGMENTS

We thank A. Nunnenkamp and J. Harris for useful comments, and O. Hart for a careful reading of the manuscript. This work was supported by the European Union's Horizon 2020 research and innovation program under Grant Agreement No. 732894 (FET Proactive HOT).

APPENDIX A: PHONON-ASSISTED PHOTON TUNNELING

In this section, we derive the Hamiltonian (1) that describes our scenario in the main text including the photon-phonon interaction term $\hat{b}\hat{a}_2^\dagger\hat{a}_1$. This term is obtained in optomechanical systems with two (or more) optical modes. Qualitatively, this term arises whenever there are two optical modes that couple to the same mechanical resonator, and the term becomes important dynamically if the mechanical frequency matches the optical frequency difference. The earliest, well-known example is the membrane-in-the-middle setup of the Harris group [58,59]. More generally, such a three-body interaction term will generically arise in systems of nonlinearly coupled modes (e.g., between three optical modes in a $\chi^{(2)}$ medium, or between microwave modes in the presence of a Josephson nonlinearity).

We consider a membrane in a cavity whose vibrational mode \hat{b} couples to two optical modes of the cavity. The position of the membrane determines the frequencies ω_L and

ω_R of the optical modes \hat{a}_L (to the left of the membrane) and \hat{a}_R (to the right of the membrane), respectively. Placing the membrane exactly in the middle of the cavity results in equal optical frequencies. Dislocating the membrane slightly from the center introduces splitting $\omega = \omega_R - \omega_L$ between the optical frequencies. Without loss of generality, we assume $\omega \geq 0$. The optical modes $\hat{a}_{L/R}$ coupled to the mechanical mode \hat{b} are described by the Hamiltonian

$$\hat{H} = \omega_L \hat{a}_L^\dagger \hat{a}_L + \omega_R \hat{a}_R^\dagger \hat{a}_R + \Omega \hat{b}^\dagger \hat{b} + J_0 (\hat{a}_L^\dagger \hat{a}_R + \text{H.c.}) - g_0 (\hat{a}_L^\dagger \hat{a}_L - \hat{a}_R^\dagger \hat{a}_R) (\hat{b}^\dagger + \hat{b}), \quad (\text{A1})$$

where Ω is the mechanical frequency, g_0 is the single-photon optomechanical coupling strength, and J_0 is the optical coupling strength. For optical modes with a different transversal spatial profile, J_0 can be arbitrarily tuned by the tilt of the membrane [59]. Due to the optical coupling, the cavity modes hybridize and that gives rise to supermodes

$$\hat{a}_1 = \frac{-J_0 \hat{a}_L + \lambda \hat{a}_R}{\sqrt{J_0^2 + \lambda^2}}, \quad (\text{A2})$$

$$\hat{a}_2 = \frac{\lambda \hat{a}_L + J_0 \hat{a}_R}{\sqrt{J_0^2 + \lambda^2}}, \quad (\text{A3})$$

at frequencies $\nu_1 = \omega_L - \lambda$ and $\nu_2 = \omega_R + \lambda$, where $\lambda = \sqrt{\frac{\omega^2}{4} + J_0^2} - \frac{\omega}{2}$. In terms of the supermodes, the Hamiltonian reads

$$\hat{H} = \sum_{j=1}^2 \nu_j \hat{a}_j^\dagger \hat{a}_j + \Omega \hat{b}^\dagger \hat{b} + [J_{\text{res}} (\hat{a}_2^\dagger \hat{a}_2 - \hat{a}_1^\dagger \hat{a}_1) + J (\hat{a}_1^\dagger \hat{a}_2 + \text{H.c.})] (\hat{b}^\dagger + \hat{b}), \quad (\text{A4})$$

where

$$J = \frac{g_0}{\sqrt{1 + \frac{\omega^2}{4J_0^2}}}, \quad (\text{A5})$$

$$J_{\text{res}} = \frac{g_0}{\sqrt{1 + \frac{4J_0^2}{\omega^2}}}. \quad (\text{A6})$$

Next, we assume driving of $\hat{a}_{L/R}$ with lasers of strengths $E_{L/R}$ at frequencies $\nu_{D,L/R}$. Neglecting quantum fluctuations around large optical amplitudes, we can derive equations of motion

$$\dot{\phi} = \Delta_M + \frac{J_{\text{res}}}{B} (|a_1|^2 - |a_2|^2) \cos[\phi - \delta t] - \frac{J}{B} \text{Re}[a_1^* a_2 e^{-i\phi} + a_1 a_2^* e^{-i\phi + 2i\delta t}], \quad (\text{A7})$$

$$\dot{a}_1 = i\Delta_1 a_1 - iE_1 - iE_1^{\text{res}} e^{-i\delta t} + iB[J_{\text{res}} a_1 (e^{-i\phi + i\delta t} + e^{i\phi - i\delta t}) - J a_2 (e^{-i\phi} + e^{i\phi - 2i\delta t})] - \frac{\kappa}{2} a_1, \quad (\text{A8})$$

$$\dot{a}_2 = i\Delta_2 a_2 - iE_2 + iE_2^{\text{res}} e^{i\delta t} - iB[J_{\text{res}} a_2 (e^{-i\phi + i\delta t} + e^{i\phi - i\delta t}) + J a_1 (e^{i\phi} + e^{-i\phi + 2i\delta t})] - \frac{\kappa}{2} a_2, \quad (\text{A9})$$

in frames rotating at suitable frequencies (mode a_1 at $\nu_{D,L}$, mode a_2 at $\nu_{D,R}$, and mode b at $\delta = \nu_{D,R} - \nu_{D,L}$), where we assume mechanical limit-cycle

oscillations $\langle \hat{b} \rangle = B e^{i\phi}$ with a fixed amplitude B . We define $\Delta_1 = \nu_{D,L} - \nu_1$, $\Delta_2 = \nu_{D,R} - \nu_2$, $\Delta_M = \delta - \Omega$, $E_1 = E_L / \sqrt{1 + \lambda^2 / J_0^2}$, $E_1^{\text{res}} = E_R / \sqrt{1 + J_0^2 / \lambda^2}$, $E_2 = E_R / \sqrt{1 + \lambda^2 / J_0^2}$, and $E_2^{\text{res}} = E_L / \sqrt{1 + J_0^2 / \lambda^2}$.

Now we consider the resonant case, $\Delta_1 = \Delta_2 = 0$, when the generation of the synthetic electric fields is the most pronounced. In this case, driving of \hat{a}_L mostly addresses supermode \hat{a}_1 , since the laser is on resonance with its frequency and the overlap of \hat{a}_L with the other supermode \hat{a}_2 is small provided that $\omega \gg J_0$. As a result, we can neglect the residual driving of the supermode \hat{a}_2 . Similarly, driving of \hat{a}_R leads to addressing mostly the supermode \hat{a}_2 . If the residual drivings are negligible and we tune the mechanical frequency such that $\Omega = \nu_2 - \nu_1$, the coupling term $\hat{b} \hat{a}_2^\dagger \hat{a}_1$ is selected and the other coupling terms in the Hamiltonian (A4) are off resonance. Neglecting the off-resonant coupling terms within the rotating-wave approximation, which is valid for $\Omega = \nu_2 - \nu_1 \approx \omega \gg \kappa, g_0, g_0 B$, the equations of motion reduce to Eqs. (2), (3), and (4) considered in the main text with the effective tunneling amplitude J given by Eq. (A5). The tunneling amplitude J decreases with decreasing J_0 . As a result, a fine tuning of the ratio ω / J_0 is necessary to achieve the optimal trade-off between eliminating the residual driving of unwanted supermodes and maximizing the amplitude of the term $\hat{b} \hat{a}_2^\dagger \hat{a}_1$.

We have derived the Hamiltonian (1) for optical supermodes, which is considered as the starting point in the main text, from the fundamental optomechanical Hamiltonian (A1) for two optical modes coupled to a single mechanical mode. In summary, whenever two optical modes and one mechanical resonator are in a mutual interaction, and when the mechanical frequency matches the optical frequency difference (at least approximately), the interaction term $\hat{a}_2^\dagger \hat{a}_1 \hat{b} + \text{H.c.}$ assumed in our work is the generic outcome.

APPENDIX B: STEADY STATES OF THE TWO-SITE SYSTEM

In this section, we analyze the steady states of the two-site system with a single mode being driven. They are stationary solutions of the equations of motion [Eqs. (2), (3), and (4) in the main text] constant in time. We first apply a time-dependent gauge transformation to express the time evolution of the mechanical phase in a form of an effective optical frequency shift. Then we find a stationary condition for the synthetic electric field \mathcal{E} . Finally, we use an effective potential for the synthetic electric field to study stability of its stationary solutions.

As mentioned in the main text, we assume that only one mode is driven. We label the driven mode by the index $k = 1, 2$. Driving strengths can then be expressed as $E_j = E \delta_{j,k}$ for $j = 1, 2$, where $\delta_{j,k}$ is the Kronecker delta. The detuning of the nondriven mode can be set to zero, since there is no driving

frequency. Therefore, the optical detunings can be expressed as $\Delta_j = \Delta_0 \delta_{j,k}$. We make use of the time-dependent gauge transformation

$$\phi = \tilde{\phi} + \chi, \quad (\text{B1})$$

$$a_1 = \tilde{a}_1 e^{-i\chi \delta_{2,k}}, \quad (\text{B2})$$

$$a_2 = \tilde{a}_2 e^{i\chi \delta_{1,k}}, \quad (\text{B3})$$

which moves the dynamics of the mechanical phase to the time-dependent gauge parameter χ . By appropriately choosing χ , we can always achieve $\tilde{\phi} = 0$. The time-dependent gauge transformation leaves the absolute values of the optical amplitudes unchanged. As a result, a particular value of the gauge parameter is irrelevant. Only its first derivative $\dot{\chi} = \dot{\phi}$ influences the optical occupations. The time evolution of the mechanical phase results in an effective shift $(\delta_{2,k} - \delta_{1,k})\dot{\chi}$ of the nondriven optical mode's frequency. Note that the driven mode, a_k , is forced to oscillate with the frequency of the laser drive, and thus it does not experience any frequency shift.

The role of the optical frequency shift $\dot{\chi}$ can be understood in analogy to electromagnetism. The mechanical phase corresponds to an effective vector potential. According to conventional electromagnetism, the time evolution of the vector potential generates an electric field. This electric field can be also represented by a scalar potential gradient. In this analogy, the time evolution of the mechanical phase generates a synthetic electric field $\mathcal{E} = \dot{\chi}$ for photons, which represent an effective optical frequency shift.

To provide the fixed-point analysis for both the cases $k = 1, 2$ at once, we use general indexes $(k, l) \in \{(1, 2), (2, 1)\}$ to label the optical modes. According to the gauge transformation (B1), (B2), and (B3), the equations of motion transform to

$$\dot{\tilde{\phi}} = \mathcal{E} - \Delta_M + \frac{J}{B} \text{Re}[\tilde{a}_k^* \tilde{a}_l] = 0, \quad (\text{B4})$$

$$\dot{\tilde{a}}_k = i\Delta_0 \tilde{a}_k - iE - iJB\tilde{a}_l - \frac{\kappa}{2} \tilde{a}_k, \quad (\text{B5})$$

$$\dot{\tilde{a}}_l = i(\delta_{2,k} - \delta_{1,k})\mathcal{E}\tilde{a}_l - iJB\tilde{a}_k - \frac{\kappa}{2} \tilde{a}_l, \quad (\text{B6})$$

where we substituted $\mathcal{E} = \dot{\chi}$. Taking the time derivative of Eq. (B4), we obtain the equation of motion for the synthetic electric field

$$\begin{aligned} \dot{\mathcal{E}} = & -\kappa(\mathcal{E} - \Delta_M) + \frac{EJ}{B} \text{Im}[\tilde{a}_l] \\ & + \frac{J}{B} [(\delta_{2,k} - \delta_{1,k})\mathcal{E} - \Delta_0] \text{Im}[\tilde{a}_k^* \tilde{a}_l]. \end{aligned} \quad (\text{B7})$$

To find stationary solutions of the equations of motion (B5), (B6), and (B7), we first use that the equations (B5) and (B6) are linear in terms of optical amplitudes. For a given value of the synthetic electric field \mathcal{E} , the stationary optical amplitudes read

$$\tilde{a}_k = E \frac{(\delta_{2,k} - \delta_{1,k})\mathcal{E} + i\frac{\kappa}{2}}{-J^2 B^2 + (\delta_{2,k} - \delta_{1,k})\mathcal{E}\Delta_0 - \left(\frac{\kappa}{2}\right)^2 + i\frac{\kappa}{2}[(\delta_{2,k} - \delta_{1,k})\mathcal{E} + \Delta_0]}, \quad (\text{B8})$$

$$\tilde{a}_l = \frac{JB}{(\delta_{2,k} - \delta_{1,k})\mathcal{E} + i\frac{\kappa}{2}} \tilde{a}_k. \quad (\text{B9})$$

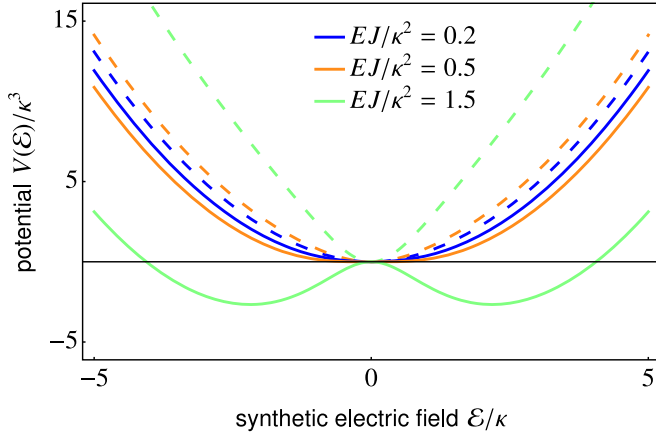


FIG. 4. The potential for the synthetic electric field. It has a single minimum at $\mathcal{E} = 0$ for $k = 2$ (dashed lines) when the higher optical frequency is driven. For $k = 1$, when the lower optical frequency is driven, the stationary value $\mathcal{E} = 0$ becomes unstable with increasing EJ/κ^2 as two minima with a finite frequency shift emerge (solid lines). (The potential is plotted for $BJ/\kappa = 0.5$.)

In the following, we set $\Delta_O = \Delta_M = 0$ to present the important features of the steady states. These features are not changed by finite detunings. We discuss the effects of finite detunings at the end of this section. By substituting the stationary values of the optical amplitudes (B8), (B9) into Eq. (B7), we obtain the stationary condition for the synthetic electric field

$$\dot{\mathcal{E}} = -\kappa \mathcal{E} \frac{\left(\frac{\mathcal{E}}{\kappa}\right)^2 + 4\left[\left(\frac{JB}{\kappa}\right)^2 + \frac{1}{4}\right]^2 + 4(\delta_{2,k} - \delta_{1,k})\left(\frac{EJ}{\kappa^2}\right)^2}{\left(\frac{\mathcal{E}}{\kappa}\right)^2 + 4\left[\left(\frac{JB}{\kappa}\right)^2 + \frac{1}{4}\right]^2} = 0. \quad (\text{B10})$$

For $k = 2$, when the mode with the higher optical frequency, a_2 , is driven, only the single stationary solution, $\mathcal{E} = 0$, exists. For $k = 1$, when the mode with the lower optical frequency, a_1 , is driven, stationary solutions with a finite synthetic electric field

$$\mathcal{E}_{\pm} = \pm 2\kappa \sqrt{\left(\frac{EJ}{\kappa^2}\right)^2 - \left[\left(\frac{JB}{\kappa}\right)^2 + \frac{1}{4}\right]^2} \quad (\text{B11})$$

emerge for $4EJ/\kappa^2 > 4(BJ/\kappa)^2 + 1$ in addition to $\mathcal{E} = 0$.

To gain intuition about the stability of these stationary solutions, we find the potential

$$V(\mathcal{E}) = \frac{\kappa^3}{2} \left(\frac{\mathcal{E}}{\kappa}\right)^2 + 2\kappa^3 (\delta_{2,k} - \delta_{1,k}) \left(\frac{JE}{\kappa^2}\right)^2 \times \ln \left\{ \left(\frac{\mathcal{E}}{\kappa}\right)^2 + 4 \left[\left(\frac{JB}{\kappa}\right)^2 + \frac{1}{4} \right]^2 \right\}, \quad (\text{B12})$$

such that $-dV(\mathcal{E})/d\mathcal{E}$ is equal to the right-hand side of Eq. (B10). The potential shows that the stationary solution $\mathcal{E} = 0$ is always a stable steady state for $k = 2$ when the optical mode with the higher optical frequency is driven (see Fig. 4). The stability of the steady state does not depend on

the system parameters. For $k = 1$, when the mode with the lower optical frequency is driven, the stability of the steady state depends on the two dimensionless parameters EJ/κ^2 and BJ/κ . The potential in Fig. 4 shows that the steady state $\mathcal{E} = 0$ is the only stationary solution and it is stable in the white region of the phase diagram depicted in Fig. 2 of the main text. It becomes unstable as the two steady states with a finite synthetic electric field emerge in the colored region of the phase diagram in Fig. 2 of the main text. Note that the potential does not provide conclusive information about the stability of the steady states because it does not take into account the dynamics of the optical modes. Therefore, the linear stability analysis was used to confirm that the stability of the steady states is determined correctly by the potential $V(\mathcal{E})$.

A finite mechanical detuning, $\Delta_M \neq 0$, detunes the phonon-assisted photon tunneling process from resonance. In this way, the mechanical detuning represents a static synthetic electric field for photons in contrast to the dynamically generated synthetic electric field \mathcal{E} . If the higher optical frequency is driven, the dynamically generated synthetic electric field \mathcal{E} acts against this static synthetic electric field and increases transmission to the lower optical frequency with the increasing laser amplitude. On the other hand, for the lower optical frequency being driven, the dynamically generated synthetic electric field detunes the tunneling process further from resonance with the increasing laser amplitude. As a result, it decreases light propagation to the nondriven optical mode. Above some threshold of the laser amplitude, the synthetic electric field bifurcates as the effective potential has two local minima. This again happens only for the lower frequency being driven.

A finite laser detuning, $\Delta_O \neq 0$, suppresses the coherent driving, which results in a smaller optical amplitude of the driven mode. For the higher optical frequency being driven, the synthetic electric field always vanishes even for a finite optical detuning. It vanishes also when the lower optical frequency is driven for small laser amplitudes. Similarly to the resonant case, the synthetic electric field bifurcates to finite values above the threshold of the laser amplitude for the lower frequency being driven. The threshold and the values of the bifurcated synthetic electric field are modified by the finite optical detuning since it changes the population and the phase of the driven optical mode. However, the qualitative features of the synthetic electric field remain the same. The synthetic electric field is generated only above threshold and only for the lower optical frequency being driven.

APPENDIX C: NUMERICAL SIMULATIONS OF THE FULL EQUATIONS OF MOTION

In this section, we present numerical simulations of the system described by the fundamental Hamiltonian (A1) when we consider the laser drive coupling to the original (uncoupled) cavity modes, out of which the supermodes are formed. In this way, we demonstrate the validity of the results presented in the main text where the description of the system is simplified by assuming that individual supermodes can be separately coupled to the laser drive.

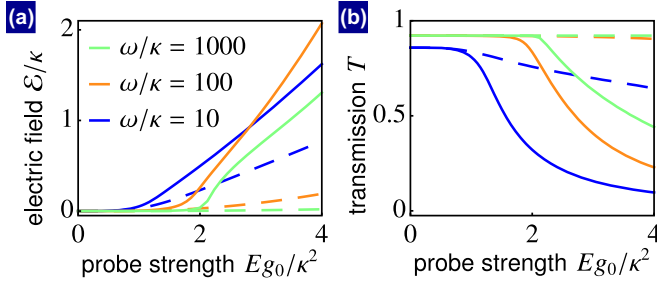


FIG. 5. Dynamically generated synthetic electric fields in the two-site system considering the model described by the fundamental Hamiltonian (A1). (a) For the uncoupled optical mode, a_L , being driven with a laser at frequency ν_1 (solid lines), a large synthetic electric field \mathcal{E} develops. For driving the uncoupled optical mode, a_R , with a laser at frequency ν_2 (dashed lines), a small synthetic electric field develops; however, it is reduced as the sideband ratio ω/κ increases (see the legend). (b) As a result, the optical transmission T to the right (solid lines) is significantly suppressed in comparison to the transmission to the left (dashed lines). In a one-dimensional array, this transmission ratio gets exponentiated by the length of the array, leading to a very significant suppression of transport in one direction. (Plotted for $Bg_0/\kappa = 2$, $J_0/\omega = 0.085$.)

We now simulate the dynamics of the uncoupled optical modes \hat{a}_L and \hat{a}_R according to the fundamental Hamiltonian (A1). To this end, we derive classical equations of motion

$$\dot{\phi} = -\Omega + \frac{g_0}{B} (|a_L|^2 - |a_R|^2) \cos \phi, \quad (\text{C1})$$

$$\dot{a}_L = i(\Delta_L + 2g_0B \cos \phi)a_L - iE_L - iJ_0a_R - \frac{\kappa}{2}a_L, \quad (\text{C2})$$

$$\dot{a}_R = i(\Delta_R - 2g_0B \cos \phi)a_R - iE_R - iJ_0a_L - \frac{\kappa}{2}a_R, \quad (\text{C3})$$

neglecting quantum fluctuations around the expectation values $a_{L/R} = \langle \hat{a}_{L/R} \rangle$, where we again assume that the mechanical mode, $\langle \hat{b} \rangle = Be^{i\phi}$, performs limit-cycle oscillation with a fixed amplitude B as well as $\Delta_L = \nu_D - \omega_L$, $\Delta_R = \nu_D - \omega_R$, and ν_D is the frequency of the laser drive. We consider driving of a single uncoupled optical mode at resonance with the corresponding supermode, i.e., $\nu_D = \nu_1$ for $E_L \neq 0$ or $\nu_D = \nu_2$ for $E_R \neq 0$, and $\Omega = \nu_2 - \nu_1$. The generated synthetic electric field and the optical transmission are shown in Fig. 5 as a function of the rescaled driving strength $E g_0/\kappa^2$. One can see in Fig. 5(a) that a large synthetic electric field is generated for mode a_L being driven (solid lines). As a result, the transmission to the right (solid lines) is significantly suppressed; see Fig. 5(b).

For driving mode a_R , a small synthetic electric field (dashed lines) is generated. This is in contrast to the simplified model in the main text, where the synthetic electric field completely vanishes when light propagates to the lower optical frequency. The small generated synthetic electric field is a result of the residual driving of the supermode a_1 due to its nonvanishing overlap with the driven uncoupled mode a_R . Since the mechanical frequency, $\Omega = \nu_2 - \nu_1$, is chosen to match the optical frequency difference, the supermode a_1 is driven on the blue sideband. However, the residual driving can be suppressed by increasing the sideband ratio ω/κ ; see Fig. 5(a). As a result, a significant suppression of the optical

transmission to the right (solid lines) in comparison to the transmission to the left (dashed lines) can be reached; see Fig. 5(b). This leads to unidirectional transport of light which works especially well in one-dimensional arrays. In such an array, the transmission ratio is exponentiated by the length of the array, which results in a large suppression of transport in one direction.

Simulating the dynamics of the uncoupled optical modes, we have shown that unidirectional light transport via synthetic electric fields is achieved for the fundamental model described by the Hamiltonian (A1). This demonstrates that the model in the main text indeed captures the important features of the interaction between the two optical modes and the mechanical mode in our scenario. Our results show that unidirectional light transport is more pronounced with the increasing sideband ratio ω/κ .

APPENDIX D: PHASE LOCKING

In this section, we provide a brief summary of phase locking, which can be reached in the two-site system by simultaneously driving both optical modes. Note that the analysis presented in the main text is for a single mode driven only. We present here quantitative features of phase locking, which has been previously well studied in a similar optomechanical system [18].

The starting point of the analysis is the equations of motion (2), (3), and (4) in the main text. The stationary values for the optical amplitudes are

$$a_1 = -\frac{JBE_2e^{-i\phi} + i\frac{\kappa}{2}E_1}{J^2B^2 + \left(\frac{\kappa}{2}\right)^2}, \quad (\text{D1})$$

$$a_2 = -\frac{JBE_1e^{i\phi} + i\frac{\kappa}{2}E_2}{J^2B^2 + \left(\frac{\kappa}{2}\right)^2}. \quad (\text{D2})$$

Note that if both optical modes are driven, the phases φ_1 and φ_2 of the laser amplitudes E_1 and E_2 , respectively, determine the phases θ_1 and θ_2 of the intracavity modes. This is different from the case when only a single optical mode is driven, where the phase of the driving amplitude is irrelevant.

The stationary value of the mechanical phase ϕ obeys the Adler equation

$$\Delta_M - |a_1||a_2| \cos(\phi - \theta) = 0, \quad (\text{D3})$$

where $\theta = \theta_2 - \theta_1$. However, the absolute values of the optical amplitudes $|a_1|$ and $|a_2|$ depend on the phase difference $\phi - \theta$. The Adler equation still determines uniquely the stationary value of $\cos(\phi - \theta)$ but the full analytical expression of this equation is complicated. Thus it is simpler to switch to the phase difference $\varphi = \varphi_2 - \varphi_1$ of the laser phases φ_1 and φ_2 . The Adler equation then has the form

$$\Delta_M - \frac{J}{B} \frac{|E_1||E_2|}{J^2B^2 + \left(\frac{\kappa}{2}\right)^2} \cos(\phi - \varphi) = 0. \quad (\text{D4})$$

We can easily read off that the stationary solution of ϕ exists for

$$|\Delta_M| \leq \frac{J}{B} \frac{|E_1||E_2|}{J^2B^2 + \left(\frac{\kappa}{2}\right)^2}. \quad (\text{D5})$$

The mechanical phase ϕ is locked under this condition to the difference φ of the laser drives' phases. Since there is one-to-one correspondence between the laser drives' phases and the intracavity modes' phases, the mechanical phase ϕ can be equivalently thought to be locked to the phase difference θ of the intracavity modes.

APPENDIX E: ONE-DIMENSIONAL ARRAYS

Here we provide details about one-dimensional arrays analyzed in the main text. We consider an array, depicted in Fig. 1(c) of the main text, represented by a stack of membranes inside a cavity. The sites of the array support optical modes a_j whose frequencies ν_j increase with site index $j = 1, \dots, n$. We assume that the phonon-assisted photon tunneling processes are resonant: $\Omega_j = \nu_{j+1} - \nu_j$, where Ω_j is the frequency of the mechanical oscillator assisting tunneling between modes \hat{a}_j and \hat{a}_{j+1} . Specifically, we will consider a situation where some optical mode $j = d$ is driven resonantly from the side, to study light propagation toward the left ($j < d$) and toward the right ($j > d$). Alternatively to membrane stacks, suitably designed coupled-cavity arrays in optomechanical crystals could implement such a setup.

The mechanical oscillators are again assumed to perform limit-cycle oscillations $\langle \hat{b}_j \rangle = B e^{i\phi_j}$ with free phases and with a fixed amplitude B equal for all mechanical oscillators. By straightforward extension of Eqs. (2), (3), and (4) (in the main text), we obtain the coupled equations of motion for the optical amplitudes and the mechanical phases

$$\dot{\phi}_j = -\frac{J}{B} \text{Re}[a_j^* a_{j+1} e^{-i\phi_j}], \quad (\text{E1})$$

$$\dot{a}_j = -iE_j \delta_{j,d} - iJB e^{-i\phi_j} a_{j+1} - iJB e^{i\phi_{j-1}} a_{j-1} - \frac{\kappa}{2} a_j, \quad (\text{E2})$$

where $\delta_{j,d}$ is the Kronecker delta. The optical modes are expressed in the frames rotating with their frequencies ν_j and the mechanical modes are in the frames rotating with the difference of optical frequencies on the neighboring sites: $\nu_{j+1} - \nu_j$.

We study the dynamics of one-dimensional arrays by numerically solving the classical equations of motion (E1) and (E2). The system converges to a steady state for any values of the parameters EJ/κ^2 and BJ/κ . Properties of the steady states are discussed in the main text.

-
- [1] M. Aspelmeyer, T. J. Kippenberg, and F. Marquardt, *Rev. Mod. Phys.* **86**, 1391 (2014).
- [2] J. Chan, T. P. M. Alegre, A. H. Safavi-Naeini, J. T. Hill, A. Krause, S. Gröblacher, M. Aspelmeyer, and O. Painter, *Nature (London)* **478**, 89 (2011).
- [3] J. D. Teufel, T. Donner, D. Li, J. W. Harlow, M. S. Allman, K. Cicak, A. J. Sirois, J. D. Whittaker, K. W. Lehnert, and R. W. Simmonds, *Nature (London)* **475**, 359 (2011).
- [4] D. J. Wilson, V. Sudhir, N. Piro, R. Schilling, A. Ghadimi, and T. J. Kippenberg, *Nature (London)* **524**, 325 (2015).
- [5] R. W. Andrews, R. W. Peterson, T. P. Purdy, K. Cicak, R. W. Simmonds, C. A. Regal, and K. W. Lehnert, *Nat. Phys.* **10**, 321 (2014).
- [6] H. Xu, D. Mason, L. Jiang, and J. G. E. Harris, *Nature (London)* **537**, 80 (2016).
- [7] S. Hong, R. Riedinger, I. Marinković, A. Wallucks, S. G. Hofer, R. A. Norte, M. Aspelmeyer, and S. Gröblacher, *Science* **358**, 203 (2017).
- [8] M. Hafezi and P. Rabl, *Opt. Express* **20**, 7672 (2012).
- [9] M. Schmidt, S. Kessler, V. Peano, O. Painter, and F. Marquardt, *Optica* **2**, 635 (2015).
- [10] A. Metelmann and A. A. Clerk, *Phys. Rev. X* **5**, 021025 (2015).
- [11] J. Kim, M. C. Kuzyk, K. Han, H. Wang, and G. Bahl, *Nat. Phys.* **11**, 275 (2015).
- [12] Z. Wang, L. Shi, Y. Liu, X. Xu, and X. Zhang, *Sci. Rep.* **5**, 8657 (2015).
- [13] F. Ruesink, M.-A. Miri, A. Alù, and E. Verhagen, *Nat. Commun.* **7**, 13662 (2016).
- [14] K. Fang, J. Luo, A. Metelmann, M. H. Matheny, F. Marquardt, A. A. Clerk, and O. Painter, *Nat. Phys.* **13**, 465 (2017).
- [15] N. R. Bernier, L. D. Tóth, A. Koottandavida, M. A. Ioannou, D. Malz, A. Nunnenkamp, A. K. Feofanov, and T. J. Kippenberg, *Nat. Commun.* **8**, 604 (2017).
- [16] S. Barzanjeh, M. Wulf, M. Peruzzo, M. Kalaei, P. B. Dieterle, O. Painter, and J. M. Fink, *Nat. Commun.* **8**, 953 (2017).
- [17] D. E. Chang, A. H. Safavi-Naeini, M. Hafezi, and O. Painter, *New J. Phys.* **13**, 023003 (2011).
- [18] G. Heinrich, M. Ludwig, J. Qian, B. Kubala, and F. Marquardt, *Phys. Rev. Lett.* **107**, 043603 (2011).
- [19] A. Xuereb, C. Genes, and A. Dantan, *Phys. Rev. Lett.* **109**, 223601 (2012).
- [20] M. Ludwig and F. Marquardt, *Phys. Rev. Lett.* **111**, 073603 (2013).
- [21] V. Peano, C. Brendel, M. Schmidt, and F. Marquardt, *Phys. Rev. X* **5**, 031011 (2015).
- [22] D. Jaksch and P. Zoller, *New J. Phys.* **5**, 56 (2003).
- [23] Y.-J. Lin, R. L. Compton, K. Jiménez-García, J. V. Porto, and I. B. Spielman, *Nature (London)* **462**, 628 (2009).
- [24] M. Aidelsburger, M. Atala, S. Nascimbène, S. Trotzky, Y.-A. Chen, and I. Bloch, *Phys. Rev. Lett.* **107**, 255301 (2011).
- [25] M. Aidelsburger, M. Atala, M. Lohse, J. T. Barreiro, B. Paredes, and I. Bloch, *Phys. Rev. Lett.* **111**, 185301 (2013).
- [26] F. D. M. Haldane and S. Raghu, *Phys. Rev. Lett.* **100**, 013904 (2008).
- [27] Z. Wang, Y. Chong, J. D. Joannopoulos, and M. Soljačić, *Nature (London)* **461**, 772 (2009).
- [28] M. Hafezi, E. A. Demler, M. D. Lukin, and J. M. Taylor, *Nat. Phys.* **7**, 907 (2011).
- [29] K. Fang, Z. Yu, and S. Fan, *Nat. Photonics* **6**, 782 (2012).
- [30] M. C. Rechtsman, J. M. Zeuner, A. Tünnermann, S. Nolte, M. Segev, and A. Szameit, *Nat. Photonics* **7**, 153 (2013).
- [31] M. Hafezi, S. Mittal, J. Fan, A. Migdall, and J. M. Taylor, *Nat. Photonics* **7**, 1001 (2013).
- [32] S. Mittal, J. Fan, S. Faez, A. Migdall, J. M. Taylor, and M. Hafezi, *Phys. Rev. Lett.* **113**, 087403 (2014).

- [33] L. M. Nash, D. Kleckner, A. Read, V. Vitelli, A. M. Turner, and W. T. M. Irvine, *Proc. Natl. Acad. Sci. USA* **112**, 14495 (2015).
- [34] R. Süssstrunk and S. D. Huber, *Science* **349**, 47 (2015).
- [35] P. Wang, L. Lu, and K. Bertoldi, *Phys. Rev. Lett.* **115**, 104302 (2015).
- [36] C. Brendel, V. Peano, O. J. Painter, and F. Marquardt, *Proc. Natl. Acad. Sci. USA* **114**, E3390 (2017).
- [37] C. Brendel, V. Peano, O. Painter, and F. Marquardt, *Phys. Rev. B* **97**, 020102(R) (2018).
- [38] A. Seif, W. DeGottardi, K. Esfarjani, and M. Hafezi, *Nat. Commun.* **9**, 1207 (2018).
- [39] N. Goldman, G. Juzeliūnas, P. Öhberg, and I. B. Spielman, *Rep. Prog. Phys.* **77**, 126401 (2014).
- [40] M. J. Hartmann, *J. Opt.* **18**, 104005 (2016).
- [41] S. Walter and F. Marquardt, *New J. Phys.* **18**, 113029 (2016).
- [42] C. N. Yang and R. L. Mills, *Phys. Rev.* **96**, 191 (1954).
- [43] P. W. Anderson, *Phys. Rev.* **130**, 439 (1963).
- [44] P. W. Higgs, *Phys. Rev. Lett.* **13**, 508 (1964).
- [45] H. Kleinert, *Gauge Fields in Condensed Matter* (World Scientific, Singapore, 1989).
- [46] C. Castelnovo, R. Moessner, and S. L. Sondhi, *Annu. Rev. Condens. Matter Phys.* **3**, 35 (2012).
- [47] P. E. Lammert, D. S. Rokhsar, and J. Toner, *Phys. Rev. Lett.* **70**, 1650 (1993).
- [48] P. E. Lammert, D. S. Rokhsar, and J. Toner, *Phys. Rev. E* **52**, 1778 (1995).
- [49] D. Banerjee, M. Dalmonte, M. Müller, E. Rico, P. Stebler, U.-J. Wiese, and P. Zoller, *Phys. Rev. Lett.* **109**, 175302 (2012).
- [50] E. Zohar, J. I. Cirac, and B. Reznik, *Rep. Prog. Phys.* **79**, 014401 (2016).
- [51] D. Marcos, P. Rabl, E. Rico, and P. Zoller, *Phys. Rev. Lett.* **111**, 110504 (2013).
- [52] D. Marcos, P. Widmer, E. Rico, M. Hafezi, P. Rabl, U. J. Wiese, and P. Zoller, *Ann. Phys.* **351**, 634 (2014).
- [53] K. E. Ballantine, B. L. Lev, and J. Keeling, *Phys. Rev. Lett.* **118**, 045302 (2017).
- [54] P. Hauke, D. Marcos, M. Dalmonte, and P. Zoller, *Phys. Rev. X* **3**, 041018 (2013).
- [55] E. A. Martinez, C. A. Muschik, P. Schindler, D. Nigg, A. Erhard, M. Heyl, P. Hauke, M. Dalmonte, T. Monz, P. Zoller, and R. Blatt, *Nature (London)* **534**, 516 (2016).
- [56] L. Yuan and S. Fan, *Phys. Rev. Lett.* **114**, 243901 (2015).
- [57] L. Yuan and S. Fan, *Optica* **3**, 1014 (2016).
- [58] J. D. Thompson, B. M. Zwickl, A. M. Jayich, F. Marquardt, S. M. Girvin, and J. G. E. Harris, *Nature (London)* **452**, 72 (2008).
- [59] J. C. Sankey, C. Yang, B. M. Zwickl, A. M. Jayich, and J. G. E. Harris, *Nat. Phys.* **6**, 707 (2010).
- [60] A. H. Safavi-Naeini and O. Painter, *New J. Phys.* **13**, 013017 (2011).
- [61] T. K. Paraíso, M. Kalaei, L. Zang, H. Pfeifer, F. Marquardt, and O. Painter, *Phys. Rev. X* **5**, 041024 (2015).
- [62] H. Wu, G. Heinrich, and F. Marquardt, *New J. Phys.* **15**, 123022 (2013).
- [63] F. Marquardt, J. G. E. Harris, and S. M. Girvin, *Phys. Rev. Lett.* **96**, 103901 (2006).
- [64] R. Lauter, C. Brendel, S. J. M. Habraken, and F. Marquardt, *Phys. Rev. E* **92**, 012902 (2015).
- [65] T. Weiss, S. Walter, and F. Marquardt, *Phys. Rev. A* **95**, 041802(R) (2017).